

Changes of the local oxygen content and ordering at twin boundaries of high- T_c $\text{YBa}_2\text{Cu}_3\text{O}_{7-x}$ superconductors

Y. Yan* and W. Y. Liang

IRC in Superconductivity, University of Cambridge, Cambridge CB3 0HE, United Kingdom

T. Walther and W. M. Stobbs†

Department of Materials Science and Metallurgy, University of Cambridge, Cambridge CB2 3QZ, United Kingdom

(Received 19 January 1996; revised manuscript received 22 August 1996)

We demonstrate here the way the local oxygen content and configuration in $\text{YBa}_2\text{Cu}_3\text{O}_{7-x}$ can be related to specific Fourier components of the image intensity in experimental high resolution electron microscopy images along the [001] zone axis. We further show that this allows us to evaluate experimentally local changes in the oxygen content and ordering at unit cell resolution in projection across twin boundaries in a high- T_c $\text{YBa}_2\text{Cu}_3\text{O}_{7-x}$ superconductor which exhibited $T_c=92$ K. Our studies indicate that, on traversing a twin boundary, there is not only an ordering change but also a reduction in the oxygen content. [S0163-1829(96)04145-8]

INTRODUCTION

The critical temperature, T_c , for $\text{YBa}_2\text{Cu}_3\text{O}_{7-x}$ depends not only on the oxygen stoichiometry, but also on the local ordering of the oxygen atoms.^{1,2} Attempts to evaluate the oxygen content and ordering using high resolution electron microscopy (HREM) are thus frequently made^{3,4} and it is well known that the imaging behavior along [100] and [010] zone axes differs depending on the oxygen content in the Cu-O chain layer. However, it was recognized from an early date⁵ that the sensitivity of an image to the degree of Cu-O chain alignment tends to be high only at relatively large thicknesses for high resolution electron microscopy. This in turn leads to doubts about the ability of a high resolution imaging method for quantitative analysis when it is required to compare intensities rather than patterns because of the contributions which can arise due to multiple inelastic/elastic scattering.⁶ It has also been recently demonstrated that the problems in this context remain even when assessing filtered images.⁷ Nonetheless there are strong motivations for finding improved methods for characterizing the local structure and O content near twin boundaries because variations in their local composition and structure can both change T_c (Refs. 8 and 9) and modify their effectiveness as pinning centers for magnetic-flux lines.^{10,11} Accordingly instead of making a comparison of full high resolution image series with simulations, we have investigated the application of specific Fourier components sensitive to the structural parameter of interest (in this case the form of the Cu-O chains). The method has been demonstrated to be very effective in the characterization of local changes in Al content in $\text{Al}_x\text{Ga}_{1-x}\text{As}$ layered systems when using the compositionally sensitive Fourier component associated with the (002) reflection.¹² Here we examine the relationship between the oxygen content in the c axis projection of a unit cell and the Fourier components in an image associated with the (100) and (010) spacings and investigate the application of the above approach to the characterization of the form of the O content change for a typical twin boundary in a high- T_c $\text{YBa}_2\text{Cu}_3\text{O}_{7-x}$ sample.

EXPERIMENTAL DETAILS

The single crystal of $\text{YBa}_2\text{Cu}_3\text{O}_{7-x}$ examined ($T_c=92$) was grown from a highly concentrated flux containing (10–15)% $\text{YBa}_2\text{Cu}_3\text{O}_x$ and (90–85)% $\text{Ba}_3\text{Cu}_7\text{O}_{10}$.¹³ Specimens for electron microscopy were prepared by the standard technique for ceramic oxides in which crystals are ground in alcohol using an agate pestle at room temperature and extracted onto a porous carbon film. The high resolution electron microscopical data described here were obtained using a JEOL 4000EX-II microscope with a point resolution of 0.17 nm. Lattice images were recorded after an observation time short enough to avoid electron beam irradiation effects.⁴ Image simulations were carried out using the EMS program software¹⁴ (parameters: acceleration voltage of 400 kV; spherical aberration of 1 mm; defocus spread of 10 nm; beam divergence of 1 mrad; sampling 0.006 nm/pixel). The HREM images were analyzed using routines written in the macro language SEMPER.¹⁵

THE FOURIER COMPONENT APPROACH FOR LOCALIZED CHANGES IN O ORDERING IN YBCO

As was first demonstrated by neutron diffraction^{16,17} two kinds of oxygen vacancies are ordered in the perfect structure: one is located at (0,0,1/2) in the Y planes, and the other is at (1/2,0,0). It is the latter which leads to the existence of a Cu-O chain along the **b** direction in the basal planes. Pendellösung plots for various lower index beams contributing to the HREM images in the [001] projection were examined for an accelerating voltage of 400 kV. These showed that for this voltage significant differences between the (100) and (010) beams, as associated with the oxygen ordering in the basal planes, are apparent for specimen thicknesses greater than 7.0 nm.^{4,5} Further analysis of simulated c-axis high resolution images reveals that a distinctive contrast feature associated with the ordering, which readily allows discrimination of the **a** and **b** directions, can be defined

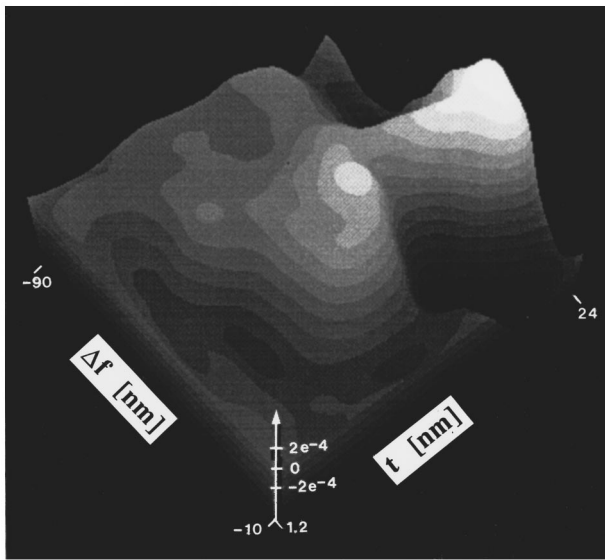


FIG. 1. Contour plot of the normalized difference of the Fourier coefficients $[U(010)-U(100)]/U(000)$ in simulated $[001]$ HREM images for various defoci and thicknesses.

as the difference in the amplitudes of the Fourier coefficients $U(010)$ and $U(100)$ of the intensity in the image as normalized by the background intensity $U(000)$. The sum of the Fourier amplitudes $U(010)$ and $U(100)$ should remain constant for the regions having perfect oxygen ordering and full oxygen content. Moreover, as can be seen from Fig. 1, the parameter is relatively insensitive to the precise defocus Δf and thickness t over reasonable ranges for each of $\Delta f \approx -30$ to -50 nm and $t \approx 9$ to 15 nm. Clearly a precise evaluation of the O content would require the comparison of the values of this parameter, as extracted from experimental images at known thicknesses and defoci, with values obtained similarly for standard specimens. This is partially because of uncertainties in the precise anisotropic form of the Debye Waller parameter to be used for O,⁵ and partially because, without energy loss filtering, contributions to the image detail due to inelastic/elastic scattering are hard to quantify.⁶ It is nonetheless interesting to examine the sensitivity of the approach, its spatial resolution and the degree to which data obtained for an interface might be affected by the Fresnel contrast associated with the discontinuity. Accordingly we now describe the results we have obtained in applying the method to the analysis of the form of the O distribution across a typical defect free planar twin boundary.

An $[001]$ HREM image of such a twin boundary, taken near Scherzer focus ($\Delta f = -40 \pm 10$ nm), is shown in Fig. 2(a) and optical diffraction patterns obtained from each of the twinned domains, I and II, are shown in Figs. 2(b) and 2(c), respectively. While the intensities of all $\{110\}$ reflections are almost identical in both twinned domains, that of the lowest index reflection in one domain is much stronger along $[010]$ than along $[100]$, and this exchanges across the boundary. It is thus clear that differences in imaging behavior across the boundary are sufficient to allow the **a** and **b** directions to be distinguished in the conventional HREM image, at least with the aid of optical diffraction. However, our interest here lies in seeing whether the localized extraction of the specific Fourier coefficients discussed above allows in-

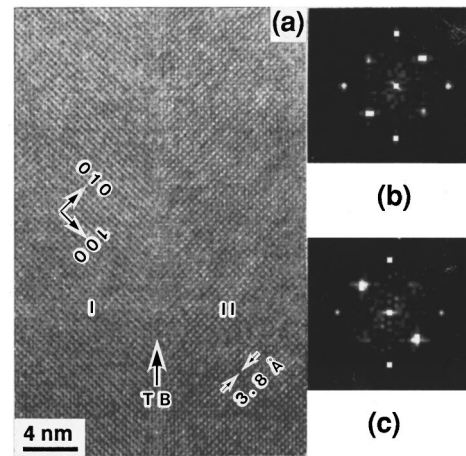


FIG. 2. (a) $[001]$ HREM image of a typical twin boundary. The optical diffraction patterns obtained from twinned domains I and II are shown in (b) and (c).

ferences to be drawn about the distance from the twin boundary over which there might be changes in the O distribution. Whether this will be the case depends primarily on whether or not there are comparable Fresnel contributions to the contrast due to the changes in projected potential at the boundary. This was examined by extracting a low pass filtered version of the top part of the original lattice image [Fig. 3(a)], as shown in Fig. 3(b). An aperture in Fourier space was used which allowed only frequencies smaller than $|g_{100}|$ to contribute. While the boundary can be weakly discerned in the image [as can be seen from the intensity distribution as projected along the boundary in Fig. 3(c)], the magnitude of the low frequency scattering contribution due to the boundary, which is of a sense indicative of a reduction in the local projected potential, is small. This is as would be expected for the low defocus used but nonetheless suggests that any change in the local projected potential at the boundary is not atomically localized. Leaving this point aside for the present, the critical point in the analysis of the use of the $U(010)$ and $U(100)$ Fourier coefficients for the localized analysis of the O distribution rests on whether or not the magnitudes of the

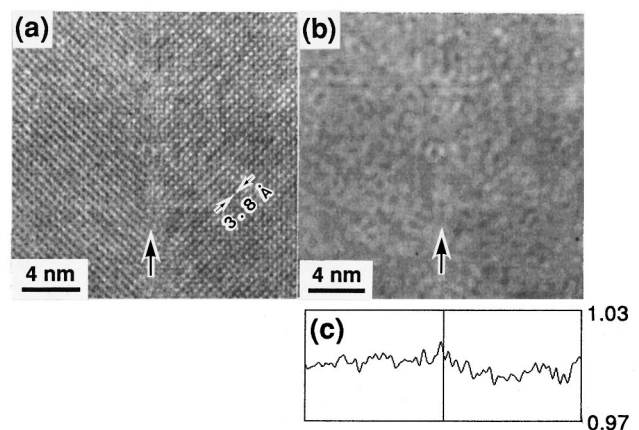


FIG. 3. (a) Enlarged top part of Fig. 2(a). (b) A low pass filtered image of (a). (c) The line scan of the low pass filtered image along the twin boundary. [The line scan in (c) is normalized with respect to the average intensity value in (a).]

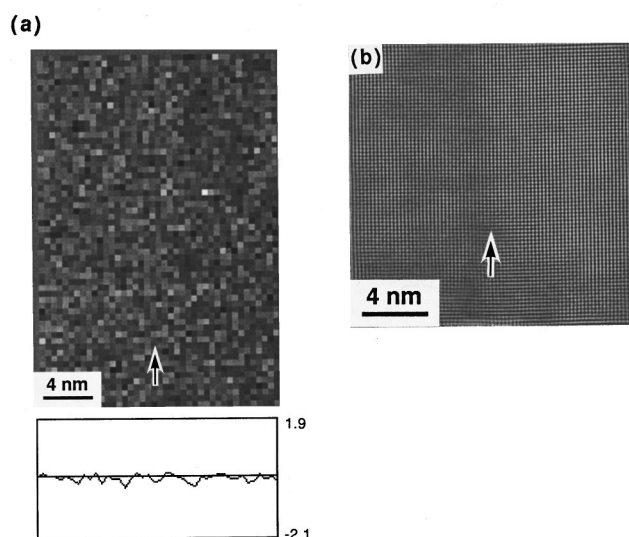


FIG. 4. (a) A two-dimensional grey level map of the signal $[U(110)-U(110)]/U(000)$ in all unit cells of Fig. 2(a). (The intensity values in the line scan are multiplied by a factor 10^5 .) (b) The $\langle 110 \rangle$ filtered lattice image of the top part of the original HREM image shown in Fig. 3(a).

changes in these coefficients at and across the boundary are significantly greater than the contrast seen in the low pass band image [Fig. 3(b)]. Preliminary examination of the changes in $U(010)$ and $U(100)$ demonstrated that this is in fact the case so we are able to proceed with the analysis of the oxygen distribution across the boundary using the comparison of these coefficients.

The analysis of the oxygen content and ordering near to the twin boundary in Fig. 2(a) is carried out by obtaining the magnitude of the specific Fourier components of the image intensity of interest for every individual unit cell as described by Walther *et al.*¹² The intensity distribution in every unit cell in Fig. 2(a) was thus resampled onto a perfect 16×16 pixels square and Fourier transformed. In the next step the amplitudes $U(\mathbf{g})$ of the Fourier coefficient of the image intensity distribution corresponding to the reciprocal lattice vectors \mathbf{g} were calculated for each of these unit cells. Figure 4(a) is a grey-level map depicting the value $[U(110) - U(110)]/U(000)$ of all unit cells from Fig. 2(a), and thus the local asymmetry in the two perpendicular sets of $\{110\}$ lattice fringes normalized by the background intensity. The $\langle 110 \rangle$ filtered lattice image¹⁸ of the top part of the original HREM image [Fig. 3(a)] is shown in Fig. 4(b). The absence of structural information in Figs. 4(a) and 4(b) means that the signal is the same in both domains and is not affected by the presence of the boundary. A significant crystal tilt across the boundary or a serious distortion of the cation sublattice would manifest themselves in such images, so we can exclude such affections as giving significant changes in the Fourier coefficients sensitive to the oxygen content.

As we have seen from Fig. 1 it is the $U(100)$ and $U(010)$ Fourier coefficients which are sensitively related to the oxygen content and distribution in the CuO chains. Figure 5(a)–5(d) are grey-level maps showing the Fourier amplitudes $U(010)/U(000)$, $U(100)/U(000)$, $[U(010) - U(100)]/U(000)$, and $[U(010) + U(100)]/U(000)$, respectively, for the unit cells from Fig. 2(a), together with line scans obtained by vertical

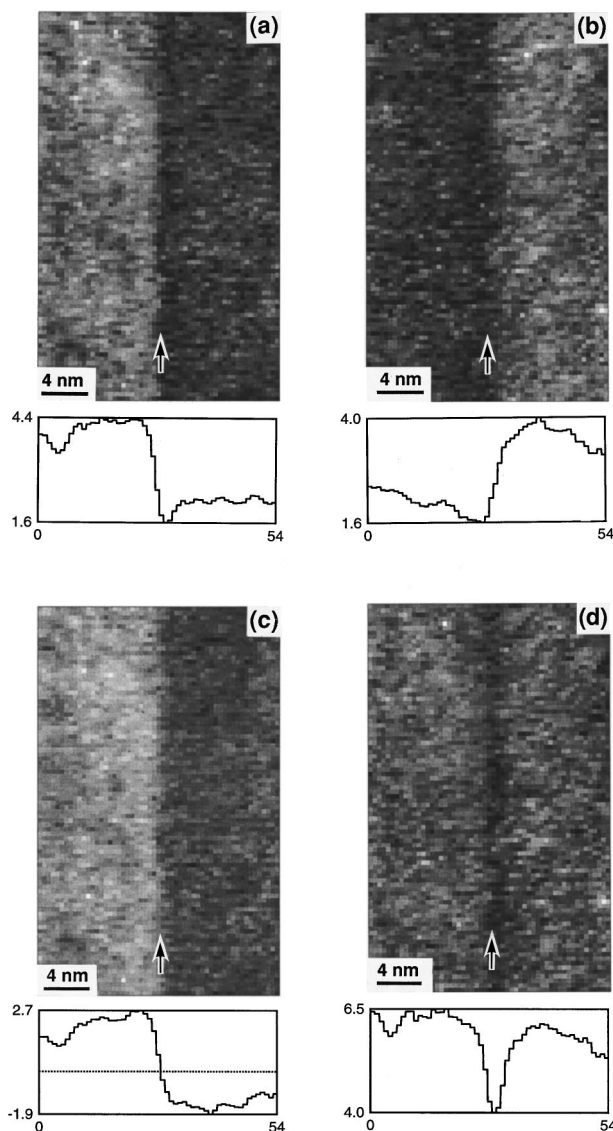


FIG. 5. Two-dimensional grey level maps of the Fourier amplitudes (a) $U(010)/U(000)$, (b) $U(100)/U(000)$, (c) $[U(010) - U(100)]/U(000)$, and (d) $[U(010) + U(100)]/U(000)$ from all unit cells in Fig. 2(a) and their line scans along the twin boundary. [The intensity values in the line scan are multiplied by a factor 10^5 . The width of each step (54 steps in total) corresponds to one unit cell: $a \approx 0.38$ nm.]

projection. The average intensity of the normalized Fourier amplitude $U(010)/U(000)$ of domain I is about two times larger than that of $U(100)/U(000)$, and vice versa for domain II. It should also be noted that the magnitude of the change is far larger than was seen at the boundary for the low pass band image [Fig. 3(c)], this confirming that the Fresnel contrast due to the boundary has insignificant effects on the use of these Fourier coefficients for the determination of any localized changes in the O distribution at the boundary. The reason for the change in the magnitude of the respective Fourier coefficients across the boundary is of course the exchange of the \mathbf{a} and \mathbf{b} axes in the twinned domains due to the Cu-O chains being rotated by 90° across the twin boundary. The line scan of Fig. 5(c) shows that the difference between the Fourier amplitudes $U(010)$ and $U(100)$ has nearly the same magnitude for both domains, with the sign being re-

versed. The small asymmetry observed is presumably due to weak astigmatism or beam tilt which would enhance the intensity of one set of $\{100\}$ lattice planes over the other. Comparing Fig. 5(c) not only with the low pass band filtered image [Fig. 3(b)] but also with the map in Fig. 4(a), we can conclude that any specimen misorientation away from the $[001]$ direction is minimal for both domains in the experimental HREM image of Fig. 2(a), and that no other effects such as metal sublattice disordering can be sufficient to produce any effects on the $U(100)$ and $U(010)$ maps which could compete with the effects on them due to the oxygen distribution. Thus the changes of the Fourier amplitudes $U(010)$ and $U(100)$ from domain I to domain II as shown in Fig. 5 suggest that we are probing the local changes in the ordering of the oxygen atoms in the Cu-O chains. It is thus significant that the sum of the Fourier amplitudes $U(010)$ and $U(100)$, as shown in Fig. 5(d), is drastically decreased locally at the boundary. As it has been demonstrated that no other effects influence the sum of the Fourier amplitudes significantly, the drop in Fig. 5(d) leads us to the conclusion that at a typical twin boundary either the average oxygen content at the CuO chain positions is reduced or the oxygen ordering is lost. Computer simulations for two different twin boundary models¹⁹ having various oxygen content and ordering have been carried out at different defocus and thickness. It has been found that the Fourier analysis method is capable of providing reliable data on determining the oxygen ordering and content. The details on the image simulations will be

given somewhere else. Furthermore Fig. 5(d) demonstrates that the width of the twin boundary, over which the oxygen content and the ordering are at least partially lost, varies significantly from place to place along the boundary. The full width at half maximum is 1.6 ± 0.2 nm which is much wider than the result (twin boundary width: 0.7 ± 0.2 nm) obtained by x-ray diffraction for the material with similar T_c .²⁰ It is possible that this indicates preferential electron beam damage at the boundary and this will be further investigated.

CONCLUSION

In summary, we have demonstrated that the oxygen content and ordering in a high- T_c $\text{YBa}_2\text{Cu}_3\text{O}_{7-x}$ superconductor can be investigated on the sub-nm scale by an analysis of specific Fourier components of the image intensity in experimental HREM images. Our study indicates that there is at least a partial loss of the oxygen content and ordering near to a typical twin boundary. Our analysis method would allow the future quantitative measurement of the oxygen content in individual unit cells (as of course averaged over the specimen thickness) by using appropriate lattice images of $\text{YBa}_2\text{Cu}_3\text{O}_{7-x}$ with known oxygen content as reference images. Finally it can be noted that while the Fresnel method could have been used, with much higher defoci, to provide data of comparable spatial accuracy perpendicular to the boundary, the Fourier coefficient approach described here allows a two-dimensional analysis.

*Present address: Materials Science Division, Argonne National Laboratory, Argonne, IL 60439.

†Deceased.

¹R. J. Cava *et al.*, *Physica C* **165**, 419 (1990).

²H. F. Poulsen, N. H. Andersen, J. V. Andersen, H. Bohr, and O. G. Mouritsen, *Nature* **349**, 594 (1991).

³Y. Yan and M. G. Blanchin, *Phys. Rev. B* **43**, 13 717 (1991).

⁴Y. Yan and M. G. Blanchin, *Physica C* **148**, 147 (1992).

⁵R. A. Camps, S. B. Newcomb, W. O. Saxton, and W. M. Stobbs, *Inst. Phys. Conf. Ser.* **90**, 299 (1987).

⁶W. M. Stobbs and W. O. Saxton, *J. Microsc.* **151**, 171 (1987).

⁷C. B. Boothroyd, R. E. Dunin-Borkowski, W. M. Stobbs, and C. J. Humphreys, in *Beam-Solid Interactions for Materials Synthesis and Characterization*, edited by D. C. Jacobson, D. Luzzi, T. F. Heinz, and M. Iwaki, MRS Symposia Proceedings No. 354 (Materials Research Society, Pittsburgh, 1995), pp. 495–500.

⁸A. A. Abrikosov, A. I. Buzdin, M. L. Kubic, and D. A. Kuptsov, *Int. J. Mod. Phys. B* **1**, 1045 (1988).

⁹M. M. Fang, V. G. Kogan, D. A. Finnemore, J. R. Clem, L. S. Chumbleyn, and D. E. Farrell, *Phys. Rev. B* **37**, 2334 (1988).

¹⁰D. Shi, S. Sengupta, J. S. Luo, C. Varanasi, and P. J. McGinn, *Physica C* **213**, 179 (1993).

¹¹H. Theuss, *Physica C* **208**, 205 (1993).

¹²T. Walther, C. J. Humphreys, M. P. Grimshaw, and A. C. Churchill, *Philos. Mag. A* **72**, 1015 (1995).

¹³C. T. Lin *et al.*, *Physica C* **242**, 195 (1995).

¹⁴P. A. Stadelmann and P. A. Buffat, *Ultramicroscopy* **21**, 131 (1987).

¹⁵W. O. Saxton, T. J. Pitt, and M. Horner, *Ultramicroscopy* **4**, 343 (1979).

¹⁶J. J. Capponi, C. Chaillout, A. W. Hewat, P. Lejay, M. Marezio, N. Nguyen, B. Raveau, J. L. Soubeyroux, J. L. Tholence, and R. Tournier, *Europhys. Lett.* **3**, 1301 (1987).

¹⁷W. I. F. David, W. T. A. Harrison, and J. M. F. Gunn, *Nature* **327**, 310 (1987).

¹⁸M. D. Roberson, J. E. Currie, J. M. Corbett, and J. B. Webb, *Ultramicroscopy* **58**, 175 (1995).

¹⁹Y. Zhu, M. Suenaga, J. Taftø, and D. O. Welch, *Phys. Rev. B* **44**, 2481 (1991).

²⁰J. Chroach and E. K. H. Salje, *Physica C* **225**, 111 (1994).